

Compositional inhomogeneities as a source of indirect noise in subsonic and supersonic nozzles

By L. Magri[†], J. O'Brien AND M. Ihme

1. Motivation and objectives

Engine-core noise in aeronautical gas-turbines is commonly divided into direct and indirect noise (Strahle 1978; Dowling & Mahmoudi 2015; Ihme 2017). Direct combustion noise is a source of self-noise, and describes the generation of acoustic pressure fluctuations by unsteady heat release in the combustion chamber (Figure 1). In contrast, indirect combustion noise represents an induced noise-source mechanism that arises from the interaction between non-acoustic perturbations exiting the combustion chamber and downstream engine components. The indirect noise generation by temperature inhomogeneities arising from hot and cold spots is referred to as entropy noise (Marble & Candel 1977*a*), and indirect noise from vorticity fluctuations is referred to as vorticity noise (Cumpsty 1979). Once sound has been generated, its propagation through the engine core depends on mean flow gradients and the geometry, which distort, diffract and reflect the acoustic propagation. Contributions of indirect noise to the overall core-noise emission have been examined theoretically and experimentally. These studies focused on separating out the contributions to noise from the (i) direct transmission and (ii) entropy noise. Different techniques have been employed to determine the transfer functions, including compact nozzle theories (Marble & Candel 1977*a*) and expansion methods (Stow *et al.* 2002; Goh & Morgans 2011; Moase *et al.* 2007; Giauque *et al.* 2012; Durán & Moreau 2013). These theoretical investigations were supported by experimental studies (Bake *et al.* 2009; Kings & Bake 2010). These studies showed that indirect combustion noise requires consideration in the analysis of engine-core noise and can exceed the contribution from direct noise under some circumstances (see, e.g., Dowling & Mahmoudi 2015).

Common to all of these previous investigations, however, is the restriction to a single-component gas mixture without considering effects of inhomogeneities in mixture composition on the indirect noise generation. In particular, compositional inhomogeneities can arise from incomplete mixing, air dilution, and variations in the combustor exhaust gas compositions. In this work, it is shown that these inhomogeneities constitute an additional indirect noise-source mechanism by deriving the differential equations. The equations for multi-component gas mixtures are considered, and compositional fluctuations are expressed as a function of the mixture fraction. By extending the work of Ihme (2017); Magri *et al.* (2016), the governing equations for non-compact nozzles are derived and discussed. The limit of the compact nozzle is taken to apply the theory and show (i) the existence of compositional noise acting as a dipole-like acoustic source and (ii) the relative importance between noise induced by entropy spots, compositional inhomogeneities and direct noise. Vorticity noise is not investigated because the nozzle is assumed to be quasi-one-dimensional.

Lastly, the physics of composition noise are examined for each combustion product,

[†] University of Cambridge, Engineering Department, Fluid Dynamics Group, UK

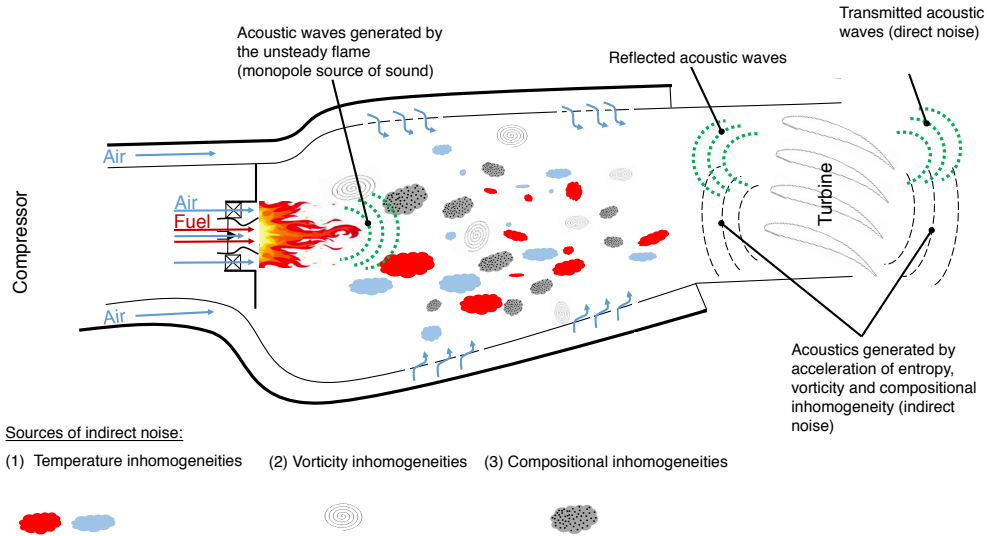


FIGURE 1. Pictorial representation of the acoustic sources in the combustion chamber of a gas turbine. Inspired by Dowling & Mahmoudi (2015).

attempting to draw a link between individual species and changes in a mixture's propensity to generate indirect noise. The sensitivity of individual species can be explained by a combination of large differences between the species and mixture's Gibbs free energy and strong gradients in product concentration with mixture fraction. However, by analyzing the species dependency of combustion products at several different mean mixture fractions, it is found that no single species dominates the noise generation over the combustor's entire range, but rather which species is the noisiest varies strongly depending on local stoichiometry.

2. Species-composition inhomogeneities generate sound

A quasi-one-dimensional nozzle flow is considered and it is assumed that (i) the flow is advection-dominated, hence, viscosity and heat/species diffusion effects are negligible; (ii) the flow is isentropic; (iii) body forces are negligible; (iv) the gas composition is parameterized in the mixture fraction space, Z ; (v) intermolecular forces are negligible (thermally perfect gas), hence, the ideal gas state equation is valid; and (vi) vibrational energy modes are negligible (calorically perfect gas), therefore, the gas constant and specific heat are functions of the mixture fraction, $R = R(Z)$, $c_p = \frac{\gamma}{\gamma-1}R(Z)$ and $\gamma = c_p/c_v$ is constant.

2.1. Governing equations

It can be shown that the problem is governed by

$$He \frac{\partial}{\partial \tau} \left\{ \frac{p'}{\gamma \bar{p}} \right\} + \tilde{u} \frac{\partial}{\partial \eta} \left\{ \frac{p'}{\gamma \bar{p}} \right\} + \tilde{u} \frac{\partial}{\partial \eta} \left\{ \frac{u'}{\bar{u}} \right\} = 0, \quad (2.1)$$

$$He \frac{\partial}{\partial \tau} \left\{ \frac{u'}{\bar{u}} \right\} + \tilde{u} \frac{\partial}{\partial \eta} \left\{ \frac{u'}{\bar{u}} \right\} + \frac{\tilde{u}}{M^2} \frac{\partial}{\partial \eta} \left\{ \frac{p'}{\gamma \bar{p}} \right\} = - \left[2 \frac{u'}{\bar{u}} - (\gamma - 1) \frac{p'}{\gamma \bar{p}} \right] \frac{\partial \tilde{u}}{\partial \eta} + \left(\frac{s'}{\bar{c}_p} + \bar{\Psi} Z' \right) \frac{\partial \tilde{u}}{\partial \eta}, \quad (2.2)$$

$$He \frac{\partial}{\partial \tau} \left\{ \frac{s'}{\bar{c}_p} \right\} + \tilde{u} \frac{\partial}{\partial \eta} \left\{ \frac{s'}{\bar{c}_p} \right\} = 0, \quad (2.3)$$

$$He \frac{\partial Z'}{\partial \tau} + \tilde{u} \frac{\partial Z'}{\partial \eta} = 0, \quad (2.4)$$

where p is the pressure; u is the velocity; s is the entropy; $\Psi = \frac{1}{c_p T} \sum_i^{N_s} \frac{\mu_i}{W_i} \frac{dY_i}{dZ}$ is the chemical potential function, where μ_i is the chemical potential, W_i is the molar mass, Y_i are the N_s species mass fractions; and $M = u/c$ is the Mach number. The non-dimensionalized variables are denoted by a tilde, the steady mean-flow quantities by a bar and the unsteady fluctuations by a prime. The axial coordinate is non-dimensionalized as $\eta = x/L$, where L is the nozzle axial length; the time as $\tau = ft$, where f is the frequency of the inlet perturbations; the mean-flow velocity as $\tilde{u} = \bar{u}/\bar{c}_a$, where \bar{c}_a is the mean-flow speed of sound at the inlet; and the mean-flow speed of sound as $\tilde{c} = \bar{c}/\bar{c}_a$. The Helmholtz number, $He = fL/\bar{c}_a$, represents the nozzle compactness with respect to acoustic perturbations, hence, $He = 0$ in compact nozzles.

A further assumption that was made in the derivation of Eqs. (2.1)-(2.4) is that the chemical potential function gradient is sufficiently small, which means that the term $\tilde{u} Z' \partial \bar{\Psi} / \partial x$ is assumed of higher order, therefore, it is neglected. The terms $[2u'/\bar{u} - (\gamma - 1)p'/\gamma \bar{p}] \partial \tilde{u} / \partial \eta$ in (2.2) represent refraction and reflection of the acoustics due to the mean-flow gradient, which can be induced by geometric variations. As already pointed out by Marble & Candel (1977b), the unsteady interaction between the entropy disturbance s' and the mean-flow gradient is a dipole-like source term. New to this analysis is the identification of the term $\bar{\Psi} Z' \partial \tilde{u} / \partial \eta$ as a second source of indirect noise, again through the action of an acoustic dipole. Physically, not only do density variations create noise through entropy mechanisms, but also differences in species generate noise through the chemical potential when mean-flow gradients are present.

2.2. Equations for the Riemann invariants

In such a flow, four integral quantities are globally conserved, which are the mass flow rate, total enthalpy, entropy and mixture fraction, respectively, and $I_{\dot{m}} = \dot{m}'/\bar{m}$, $I_{h_T} = h'_T/\bar{h}_T$, $I_s = s'/\bar{c}_p$, $I_z = Z'$. It is useful to express these invariants in terms of the compact-nozzle invariants, which are denoted with the superscript C . Due to the mean flow gradients, it can be shown that $I_{h_T}^C \neq I_{h_T}$, $I_{\dot{m}}^C \neq I_{\dot{m}}$. On the other hand, the entropy and mixture fraction invariants are the same as those in the compact nozzle $I_s = I_s^C$ and $I_z = I_z^C$. The invariants of the non-compact nozzle and the compact configuration are the same as the mean-flow gradients tend to zero. Therefore, in a general non-compact nozzle, the compact-nozzle invariants are functions of time and space. Assuming that the flow is forced harmonically at non-dimensional frequency He , the equations can be

recast in terms of the compact-nozzle invariants, yielding

$$2\pi i H e \hat{\mathbf{q}} = \mathbf{E}(\eta) \frac{\partial \hat{\mathbf{q}}}{\partial \eta}, \quad (2.5)$$

where $i^2 = -1$, $\mathbf{q} = [I_m^C, I_{h_T}^C, I_s^C, I_z^C]^T$, $\mathbf{q}(\tau, \eta) = \hat{\mathbf{q}}(\eta) \exp(2\pi i H e \tau)$ and

$$\mathbf{E}(\eta) = -\tilde{u} \begin{bmatrix} 1 & 1 + \frac{(\gamma-1)}{2} \bar{M}^2 & \frac{-1}{(\gamma-1)\bar{M}^2} & \frac{-\bar{\Psi}}{(\gamma-1)\bar{M}^2} \\ \frac{\gamma-1}{1 + \frac{\gamma-1}{2} \bar{M}^2} & 1 & \frac{\gamma-1}{1 + \frac{\gamma-1}{2} \bar{M}^2} & \frac{\gamma-1}{1 + \frac{\gamma-1}{2} \bar{M}^2} \bar{\Psi} \\ 0 & 0 & 1 & 0 \\ 0 & 0 & 0 & 1 \end{bmatrix}. \quad (2.6)$$

3. The compact-nozzle limit

In the compact-nozzle limit $He \rightarrow 0$, the total enthalpy, mass flow rate, and entropy invariants read, respectively

$$I_{h_T}^C = \frac{1}{1 + \frac{\gamma-1}{2} \bar{M}^2} \left[\frac{dT'}{\bar{T}} + (\gamma-1) \frac{\bar{M}}{\bar{c}} du' + \frac{dc_p/dZ}{\bar{c}_p} dZ' \right], \quad (3.1a)$$

$$I_m^C = \frac{d\rho'}{\bar{\rho}} + \frac{du'}{M\bar{c}}, \quad (3.1b)$$

$$I_s^C = \frac{dT'}{\bar{T}} - \frac{\gamma-1}{\gamma} \frac{dp'}{\bar{p}} + \left(\frac{dc_p/dZ}{\bar{c}_p} - \bar{\Psi} \right) dZ'. \quad (3.1c)$$

As $He \rightarrow 0$, by integration, (2.5) automatically provides the jump conditions across the nozzle

$$[[I_m^C]]_a^b = 0, \quad [[I_{h_T}^C]]_a^b = 0, \quad [[I_s^C]]_a^b = 0, \quad [[I_z^C]]_a^b = 0, \quad (3.2)$$

where the subscripts a and b denote the conditions at the inlet and outlet of the nozzle, respectively (Figure 2). In a choked nozzle, the variables are constrained by the condition that the mass flow rate attains a maximum, which yields the additional condition

$$\frac{ds'}{2\bar{c}_p} + \frac{1}{2} \bar{\Psi} dZ' - \frac{du'}{\bar{u}} + \frac{\gamma-1}{2\gamma} \frac{dp'}{\bar{p}} = 0. \quad (3.3)$$

Note that the temperature fluctuation, T' , can be expressed in terms of the other variables through the linearized equation of state

$$\frac{p'}{\bar{p}} = \frac{dR/dZ}{\bar{R}} + \frac{\rho'}{\bar{\rho}} + \frac{T'}{\bar{T}}, \quad (3.4)$$

where $(dR/dZ)/\bar{R} = (dc_p/dZ)/\bar{c}_p$ because of assumption (vi) in Section 2. By employing a characteristic decomposition of the governing equations, four independently evolving solutions at each side of the nozzle are identified, as shown in Figure 2. They correspond

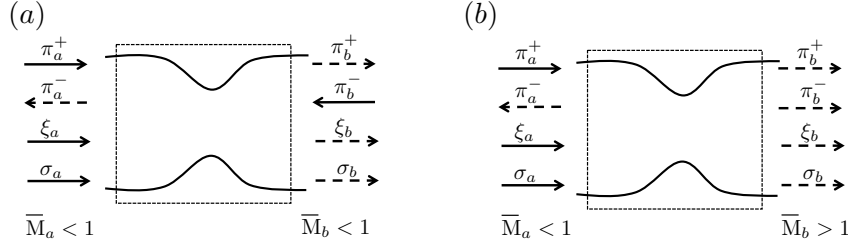


FIGURE 2. Acoustic wave, π , entropy spot, σ , compositional blob, ξ , decomposition in a (a) subcritical nozzle and (b) supercritical nozzle. Incoming quantities are denoted by solid arrows, outgoing quantities are denoted by dashed arrows.

	Subcritical nozzle	Supercritical nozzle
π_b^+/π_a^+	$\frac{2(1 + \bar{M}_a)\bar{M}_b}{(1 + \bar{M}_b)(\bar{M}_a + \bar{M}_b)} \frac{[2 + (\gamma - 1)\bar{M}_b^2]}{[2 + (\gamma - 1)\bar{M}_a\bar{M}_b]}$	$\frac{2 + (\gamma - 1)\bar{M}_b}{2 + (\gamma - 1)\bar{M}_a}$
π_b^+/σ_a	$\frac{(\bar{M}_b - \bar{M}_a)\bar{M}_b}{(1 + \bar{M}_b)[2 + (\gamma - 1)\bar{M}_a\bar{M}_b]}$	$\frac{1}{2} \frac{\bar{M}_b - \bar{M}_a}{2 + (\gamma - 1)\bar{M}_a}$
π_b^+/ξ_a	$\frac{(\gamma - 1)(\bar{\Psi}_b - \bar{\Psi}_a)[2 + (\gamma - 1)\bar{M}_b^2]\bar{M}_a\bar{M}_b}{(\gamma - 1)(1 + \bar{M}_b)(\bar{M}_a + \bar{M}_b)[2 + (\gamma - 1)\bar{M}_a\bar{M}_b]}$ $+\frac{\bar{M}_b[2(\bar{\Psi}_a - \bar{\Psi}_b) + (\gamma - 1)(\bar{\Psi}_a\bar{M}_b^2 - \bar{\Psi}_b\bar{M}_a^2)]}{(\gamma - 1)(1 + \bar{M}_b)(\bar{M}_a + \bar{M}_b)[2 + (\gamma - 1)\bar{M}_a\bar{M}_b]}$	$\frac{1}{2(\gamma - 1)} \times$ $\left[-\bar{\Psi}_b + \frac{2 + (\gamma - 1)\bar{M}_b}{2 + (\gamma - 1)\bar{M}_a} \bar{\Psi}_a \right]$

TABLE 1. Transfer functions for subcritical and supercritical nozzles. The transfer functions π_b^+/π_a^+ and π_b^+/σ_a were derived by Marble & Candel (1977a) and the compositional noise transfer functions π_b^+/ξ_a by Magri *et al.* (2016).

to the downstream and upstream propagating acoustic waves, advected entropy spot and compositional blob, respectively, $\pi^\pm = 1/2 [dp'/(\gamma\bar{p}) \pm du'/\bar{c}]$, $\sigma = ds'/\bar{c}_p$, and $\xi = dZ'$.

A nozzle transfer function is defined as the ratio between a single output (effect), such as an outgoing acoustic wave, and a single input (cause), such as an incoming entropy spot or compositional blob. Possible outputs/inputs are denoted by solid/dashed lines in Figure 2. The resulting expressions are presented in Table 1 (Magri *et al.* 2016).

4. Compositional vs. entropy noise for an n -dodecane mixture

By definition, the chemical potential of the substance i is the partial derivative of the Gibbs energy, G , with respect the number of moles of the same substance, i.e., $\mu_i = (\partial G/\partial N_i)_{T,p,n_j \neq i}$. The chemical potential function, Ψ , is calculated by finite differences from flamelet calculations $\Psi = \frac{1}{c_p T} \sum_i \frac{\mu_i}{W_i} \frac{dY_i}{dZ} = \frac{1}{c_p T} \frac{dg}{dZ}$, where g is the specific Gibbs energy (see Section 5 for more details).

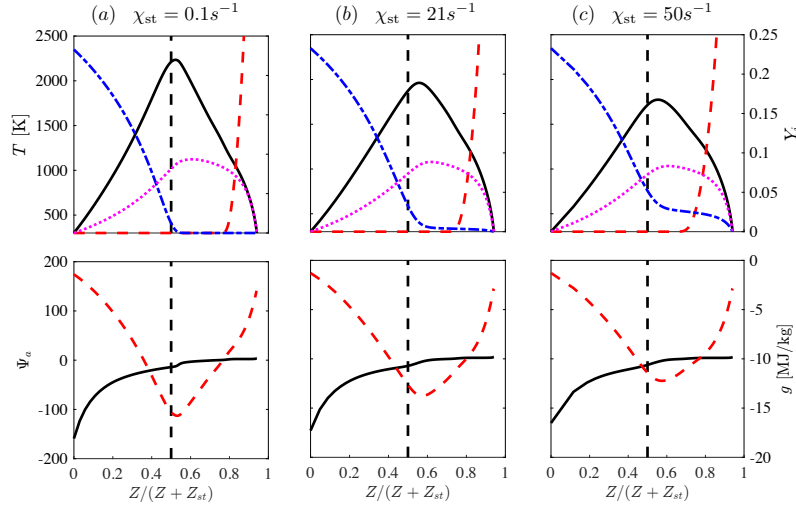


FIGURE 3. Representation of one-dimensional diffusion flame in mixture-fraction composition space for three different scalar dissipation rates; first row: flame structure, showing temperature T (solid black lines), oxygen mass fraction Y_{O_2} (blue dot-dashed lines), n -dodecane mass fraction $Y_{C_{12}H_{26}}$ (red dashed lines), and water mass fraction Y_{H_2O} (magenta dotted lines); second row: chemical potential function $\bar{\Psi}_\alpha$ (solid black lines) and specific Gibbs energy of the mixture, $g = \sum \frac{\mu_i}{W_i} Y_i$ (dashed red lines). Z_{st} is the stoichiometric mixture fraction; operating conditions: $C_{12}H_{26}/air$ combustion, $T_{fuel} = T_{ox} = 295$ K, $\bar{p} = 1$ bar (Magri *et al.* 2016).

We consider an idealized configuration in which the combustor exhaust-gas composition enters the nozzle. This exhaust-gas composition is represented from the solution of a series of one-dimensional strained diffusion flames that include the equilibrium composition, typically observed at low-power cruise conditions, and highly strained combustion conditions representative of high-load operation. The flame solutions are generated by considering n -dodecane ($C_{12}H_{26}$), a kerosene surrogate, as fuel and air in the oxidizer stream at operating conditions of 295 K and ambient pressure. The flame structure is parameterized by mixture fraction, with $Z = 0$ corresponding to the oxidizer stream and $Z = 1$ corresponding to the pure fuel stream. The flame structure is obtained from the steady-state solution of conservation equations for continuity, species, and energy, which are solved using the CANTERA software package (Goodwin 1998). The reaction chemistry is described by a 24-species mechanism (Vie *et al.* 2015).

The degree of straining, i.e., the deviation from equilibrium, is characterized by the scalar dissipation rate, χ , which is evaluated at stoichiometric condition, corresponding to a value of $Z_{st} = 0.063$. Three physically significant operating conditions are considered (a) $\chi_{st} = 0.1 s^{-1}$ (quasi-unstrained condition near equilibrium), (b) $\chi_{st} = 21 s^{-1}$ (an intermediately strained flame condition), and (c) $\chi_{st} = 50 s^{-1}$ (highly strained flame at condition near extinction). The structure of each flame together with the chemical potential function and specific Gibbs energy is shown in Figure 3. The results are presented as a function of the transformed mixture-fraction coordinate $(1 + Z_{st}/Z)^{-1}$, which divides the plot evenly between lean ($Z < Z_{st}$) and rich ($Z > Z_{st}$) conditions. The chemical potential function Ψ can reach values $\sim O(10 - 100)$, with Ψ largest on the lean side of the flame (Figure 3). These flame solutions can be interpreted as an idealized representation of the gas composition exiting the combustor. The combustor operates at a global equivalence

$\chi_{st} = 0.1 \text{ s}^{-1}$

$\chi_{st} = 21 \text{ s}^{-1}$

$\chi_{st} = 50 \text{ s}^{-1}$

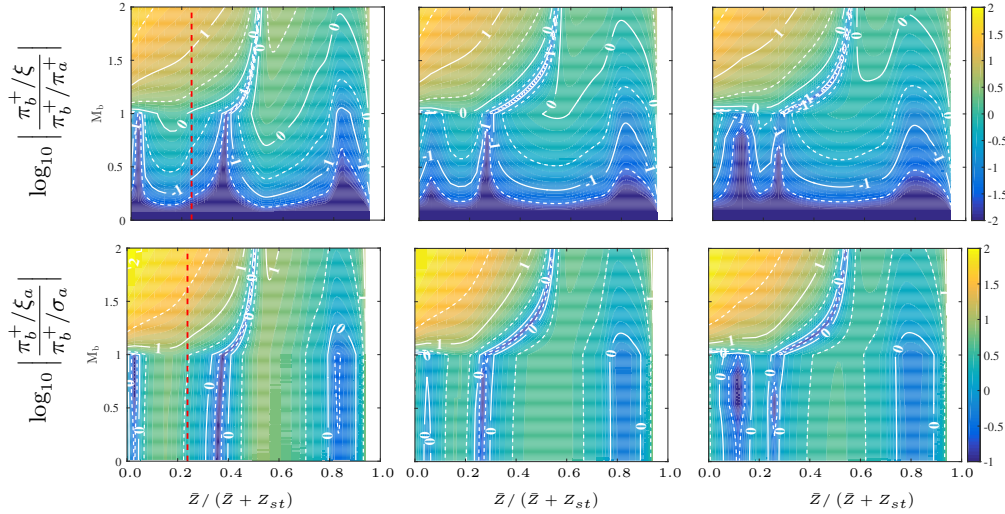


FIGURE 4. Transfer function ratios for (first row) compositional noise to direct noise and (second row) compositional noise to entropy noise. The vertical red dashed line indicates the condition of equivalence ratio of $\phi = 0.3$ (Magri *et al.* 2016).

ratio ϕ corresponding to a mean mixture fraction Z , with $Z = \phi Z_{st} / [Z_{st}(\phi - 1) + 1]$, and the corresponding thermochemical state is then taken from the flame solution of Figure 3.

To assess the compositional noise that is generated, the combustor exhaust composition for a given value of Z is isentropically compressed through an ideal nozzle, keeping the mean mixture composition frozen at this flame state. Without loss of generality, it is assumed that $M_a = 0$ (higher inlet Mach numbers were tested and the results did not change appreciably).

The transfer function ratios between compositional noise, direct noise, and entropy noise for different nozzle flows and combustor exhaust compositions are presented in Figure 4, which shows the ratio of the transfer functions between compositional and direct noise and between compositional and entropy noise, respectively, for an ideally expanded compact nozzle.

First, the transfer function for the compositional noise depends on the nozzle-exit condition, gas composition and dissipation rate. This is most pronounced for fuel-lean and supersonic conditions. The dependence of the compositional noise on the gas mixture at fuel-lean conditions is relevant to aero-engines because it corresponds to the typical operating regime of modern gas-turbine engines. This sensitivity is a direct result of stronger variations of the mixture composition and inherent differences in the chemical potential at fuel-lean conditions. This suggests that variations in the equivalence ratio, for instance during the engine operation or the consideration of low-emission combustor concepts, can lead to noise modulation by induced compositional noise, in addition to direct and entropy noise.

Second, increasing the scalar dissipation rate has effects that are noticeable in fuel-lean conditions. This is physically attributed to the leakage of reactants and incomplete combustion, which reduces the chemical potential function. Figure 3 shows the variation

of the chemical potential function as well as the specific Gibbs energy as a function of the mixture fraction. The variation in g , and correspondingly the magnitude of Ψ , are largest at fuel-lean conditions. While this broadening effect is most easily seen in physical space, it also has a weaker sensitivity in mixture fraction space, leading to the differences with respect to χ_{st} . At extreme temperatures and pressures, where dissociation of diatomic gases occurs, the sensitivity to the thermodynamic state is likely to be much stronger.

Third, to connect these results to practical applications, we provide an estimate of the ratio of composition noise to entropy noise by multiplying the corresponding transfer function ratios with the factor $\xi_a/\sigma_a = \delta Z_a/(\delta T_a/T_a)$. This factor is estimated by considering that the mixture composition at the combustor exit reaches equilibrium with a mean temperature of $T_a = 1085$ K, corresponding to an equivalence ratio of $\phi_a = 0.3$ and mean mixture fraction of $Z_a = 0.0197$ at conditions shown in Figure 3(a). The mixture-fraction distribution at the combustor exit is represented, to a first approximation, by a beta-distribution, $\beta(Z)$. The fluctuation magnitude is estimated as $\delta Z_a = \sqrt{\zeta Z_a(1 - Z_a)}$, where $\zeta \in [0, 1]$ is a coefficient for the mixedness (Dimotakis & Miller 1990). In a combustor in which the mixing is nearly completed with $\zeta = 10^{-4}$, the temperature fluctuation can be evaluated from

$$\delta T_a = \sqrt{\int_0^1 [T(Z) - T_a]^2 \beta(Z) dZ}, \quad (4.1)$$

where $T(Z)$ is the flame solution from Figure 3(a). Hence, one finds that $\xi_a/\sigma_a = 0.015$, indicating that the noise ratio at subsonic condition is below $\sim O(10^{-1})$. However, this ratio increases to values of $\sim O(1)$ in supercritical nozzles, as shown by the red dashed lines in Figure 4. This suggests that the compositional noise can become a relevant contributor to indirect combustion noise at these conditions, especially in nozzles with a shock wave in the divergent section (Magri *et al.* 2016).

5. Identification of acoustically efficient species

The previous sections have focused on compositional noise at the mixture level. This section explores the relationship between the chemical properties of individual species and the amount of indirect noise produced. While the transfer functions in Table 1 present predictions for the magnitude of compositional noise generated, they do not show how differences between species concentrations and properties give rise to indirect noise.

The impact of species chemistry is introduced via the term $\Psi = (1/c_p T) \sum_{i=1}^{N_s} (\mu_i/W_i) Y_i$ in the transfer functions, which effectively represents the mixture's normalized chemical potential on a mass basis. Since the chemical potential μ is a term that is not often reported in the literature, an alternative expression for Ψ , based on the Gibbs free energy of a mixture

$$\Psi = \frac{1}{c_p T} \left. \frac{\partial g(T, p)}{\partial Z} \right|_{T, p} = \frac{1}{c_p T} \sum_{i=1}^{N_s} g_i(T, p) \frac{\partial Y_i}{\partial Z}. \quad (5.1)$$

Analysis of the transfer functions shows that it is differences in the chemical term $\Delta\Psi$ across the nozzle that generate pressure fluctuations, so (5.1) indicates that it is largely differences in Gibbs free energy Δg_i across the nozzle and strong species gradients $\partial Y_i/\partial Z$ that generate large changes in Ψ and compositional indirect noise.

To probe the mechanism's sensitivity to individual species, the case of a single dodecane-air flamelet is examined in detail. Specifically, three points along a $\chi = 1.0$ s⁻¹ flamelet

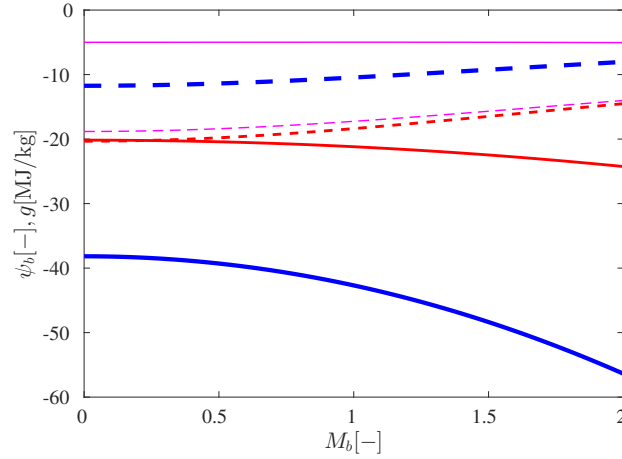


FIGURE 5. Variation of chemical effects term Ψ (solid lines) and mass-specific mixture Gibbs free energy g (dashed lines) along the isentrope corresponding to acceleration from a stagnation condition taken from the dodecane-air flame. The thick, intermediate, and thin lines correspond to normalized mixture fractions of $Z^* = 0.3, 0.5,$ and 0.7 , respectively.

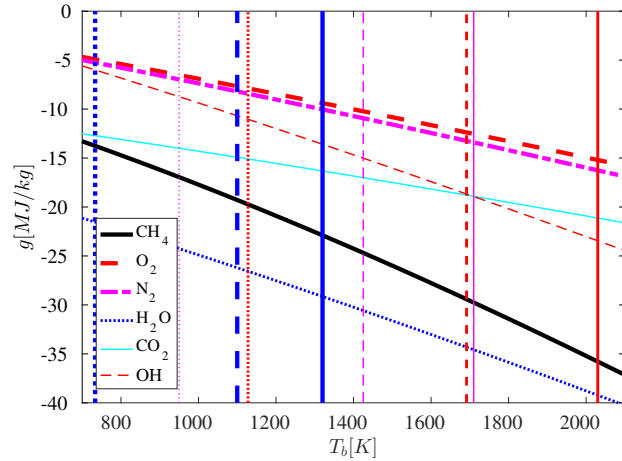


FIGURE 6. Variation in species-specific Gibbs free energy g_i for common combustion species and radicals in a dodecane-air flame vs. temperature at $p = 1$ bar. Solid, broken, and dotted vertical lines indicate the temperatures corresponding to $M = \{0, 1, 2\}$ with thick, intermediate, and thin lines corresponding to lean, stoichiometric and rich conditions, respectively.

solution were chosen for additional analysis, $Z^* = \{0.3, 0.5, 0.7\}$, corresponding to lean, stoichiometric, and rich conditions, respectively. Figure 5 shows the variation of the composition term Ψ as well as the mixture Gibbs free energy for each operating condition. For the lean case, taken from a high-response region, it can be seen that there are strong variations in g ($\approx 40\%$ from $M_a = 0$ to $M_b = 2$) which contribute to the $\Delta\Psi$ term that drives the composition noise. For the stoichiometric and rich cases, the Gibbs free energy changes less drastically and, correspondingly, both $\Delta\Psi$ and the acoustic response are much lower.

To relate these changes to individual species, Figure 6 shows the variation of species-specific Gibbs free energy versus temperature for common species. (The pressure depen-

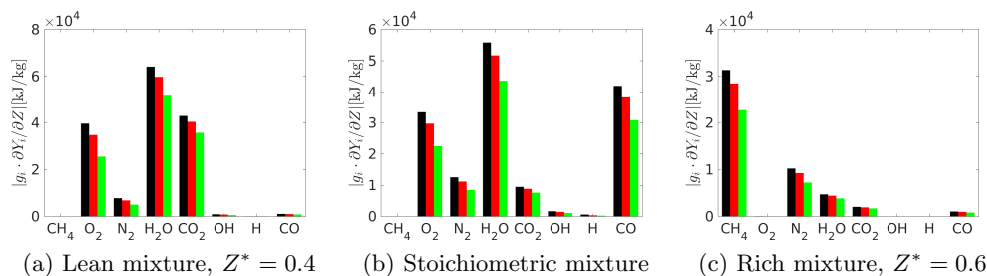


FIGURE 7. Contribution of the ten most dominant species to Ψ , $\partial Y_i / \partial Z \cdot g_i$, at different mean mixture fractions. Black bars (leftmost) correspond to the stagnation condition, red (center) to an isentropic acceleration from stagnation to $M_b = 1$, and green (right) bars to $M_b = 2.0$. Non-monotonicity in bar height vs M_b generally indicates a change in sign for that species' contribution.

dence of g_i is neglected in this figure since it is known to be relatively weak.) The figure indicates that the major components of air, O_2 and N_2 , are relatively acoustically inefficient since their Gibbs free energies are much less sensitive than other common species. Among combustion products, it can be seen that H_2O is substantially more efficient than CO_2 while the fuel is also an efficient species. Radicals such as OH and H are also potentially strong sources of noise; the variation of g_H is so strong that it could not be shown on the same scale as the other species.

However, strong gradients in a species' g_i alone are not sufficient to produce indirect noise; the relative abundance of these components must also be taken into account. Equation (5.1) indicates that large values of both $\partial g_i / \partial M_b$ and strong composition gradients $\partial Y_i / \partial Z$ must both be present to generate noise. For example, the radical H has much stronger variation in its mass-specific Gibbs free energy than those of other molecules, but, due to the chemical instability of the species, it is unlikely to be found at meaningful concentrations regardless of mixture fraction, and therefore cannot generate much indirect noise. Conversely, the Gibbs free energies of O_2 and N_2 vary quite weakly with temperature, but since O_2 is consumed and N_2 does not diffuse appreciably to the rich side of the flame, the mass fraction gradients of these species, $\partial Y_i / \partial Z$, are large enough that even their small differences in g_i over the expansion produce appreciable noise. Thus, to more quantitatively identify each species' contribution to the indirect noise, Figure 7 shows the weighted contribution of each major species to the chemical effects term Ψ or $\partial Y_i / \partial Z \cdot g_i$.

One major feature of Figure 7 is that, in reacting flows, there does not appear to be a single species which dominates the production of indirect noise. Instead, the most acoustically efficient species is a strong function of the mixture stoichiometry, just as overall noise production varies strongly with Z . For lean mixtures, both O_2 (which is being rapidly consumed) and H_2O (which is being rapidly produced) are the strongest components of composition noise while at rich conditions neither of these molecules produces appreciable noise. Likewise, dodecane is the dominant noise producer for rich mixtures, but because it is not (appreciably) present on the lean side of the flame, it has effectively no impact on noise generation near or below stoichiometric values of Z . From this, it can be concluded that analysis of the composition noise mechanism must account for both a device's intended fuel type and stoichiometry; predictions that only account for fuel choice will unlikely be accurate over a range of operating conditions.

6. Conclusions

By modelling inhomogeneities in the gas composition exiting the combustor and entering a nozzle, the compositional noise is identified as a source of indirect combustion noise, acting as an acoustic dipole. To describe this source mechanism, the nozzle theory is extended to consider a multi-component gas mixture and the chemical potential function to non-compact nozzles. This theory is applied to subcritical and supercritical nozzle flows in the limit of negligible Helmholtz numbers. It is found that the compositional noise exhibits strong dependence on the mixture composition, and can become comparable to – and even exceed – direct noise and entropy noise for supercritical nozzles and lean mixtures. The case of a dodecane-air flame is examined in detail to identify the individual combustion products that contribute most strongly to the acoustic response. It is found that no single species is responsible for this effect, but, rather, the most acoustically efficient compound varies with mixture stoichiometry. Independent of stoichiometry, however, it is seen that species which have high mass fractions, high mass fraction gradients, and whose molecular weight deviates most strongly from that of the background mixture are most acoustically efficient. This work suggests that compositional noise may require consideration with the implementation of low-emission combustors, high power-density engine cores, or compact burner concepts.

Acknowledgments

NASA with award number NNX15AV04A and the Ford-Stanford Alliance project #C2015-0590 are gratefully acknowledged for financial support. The first author is supported by the Royal Academy of Engineering Research Fellowships Scheme.

REFERENCES

- BAKE, F., RICHTER, C., MÜHLBAUER, C., KINGS, N., RÖHLE, I., THIELE, F. & NOLL, B. 2009 The entropy wave generator (EWG): A reference case on entropy noise. *J. Sound Vib.* **326**, 574–598.
- CUMPSTY, N. A. 1979 Jet engine combustion noise: Pressure, entropy and vorticity perturbations produced by unsteady combustion or heat addition. *J. Sound Vib.* **66**, 527–544.
- DIMOTAKIS, P. E. & MILLER, P. L. 1990 Some consequences of the boundedness of scalar fluctuations. *Phys. Fluids* **2**, 1919–1920.
- DOWLING, A. P. & MAHMOUDI, Y. 2015 Combustion noise. *Proc. Combust. Inst.* **35**, 65–100.
- DURÁN, I. & MOREAU, S. 2013 Solution of the quasi-one-dimensional linearized Euler equations using flow invariants and the Magnus expansion. *J. Fluid Mech.* **723**, 190–231.
- DURÁN, I., MOREAU, S. & POINSOT, T. 2013 Analytical and Numerical Study of Combustion Noise Through a Subsonic Nozzle. *AIAA J.* **51**, 42–52.
- GIAUQUE, A., HUET, M. & CLERO, F. 2012 Analytical analysis of indirect combustion noise in subcritical nozzles. *J. Eng. Gas Turbines Power* **134**, 1–8.
- GOH, C. S. & MORGANS, A. S. 2011 Phase prediction of the response of choked nozzles to entropy and acoustic disturbances. *J. Sound Vib.* **330**, 5184–5198.
- GOODWIN, D. G. 1998 CANTERA: An open-source, object-oriented software suite for combustion.

- IHME, M. 2017 Combustion and engine-core noise. *Annu. Rev. Fluid Mech.* **49** (In Press).
- KINGS, N. & BAKE, F. 2010 Indirect combustion noise: Noise generation by accelerated vorticity in a nozzle flow. *Int. J. Spray Combust. Dyn.* **2**, 253–266.
- MAGRI, L., O'BRIEN, J. & IHME, M. 2016 Compositional inhomogeneities as a source of indirect combustion noise. *J. Fluid Mech.* **799**, R4.
- MARBLE, F. E. & CANDEL, S. M. 1977*a* Acoustic disturbance from gas non-uniformities convected through a nozzle. *J. Sound Vib.* **55**, 225–243.
- MARBLE, F. E. & CANDEL, S. M. 1977*b* Acoustic disturbance from gas non-uniformities convected through a nozzle. *J. Sound Vib.* **55**, 225–243.
- MOASE, W. H., BREAR, M. J. & MANZIE, C. 2007 The forced response of choked nozzles and supersonic diffusers. *J. Fluid Mech.* **585**, 281–304.
- STOW, S. R., DOWLING, A. P. & HYNES, T. P. 2002 Reflection of circumferential modes in a choked nozzle. *J. Fluid Mech.* **467**, 215–239.
- STRAHLE, W. C. 1978 Combustion noise. *Prog. Energy Combust. Sci.* **4**, 157–176.
- VIE, A., FRANZELLI, B., GAO, Y., LU, T., WANG, H. & IHME, M. 2015 Analysis of segregation and bifurcation in turbulent spray flames: A 3D counterflow configuration. *Proc. Combust. Inst.* **35**, 1675–1683.